Heliyon 10 (2024) e33837

Contents lists available at ScienceDirect

Heliyon

journal homepage: www.cell.com/heliyon

Research article

$CaCO_3$-Encapsulated polydopamine with an adsorbed TLR7 agonist for improved tumor photothermal immunotherapy

RuYan Li [a], XianDong Shi [a], JingYi Zhang [a], BaoQing Liu [a], Jian Shen [b], HaiLong Liu [a,*], JiaHong Zhou [a,**]

[a] College of Life Sciences, Nanjing Normal University, Nanjing, 210023, China
[b] College of Chemistry and Materials Science, Jiangsu Key Laboratory of Biofunctional Materials, Nanjing Normal University, Nanjing, 210023, China

ARTICLE INFO

Keywords:
Drug delivery nanosystem
Polydopamine
Calcium carbonate
TLR7 agonist
Photothermal immunotherapy

ABSTRACT

Because of the tumor's recurrence and significant metastasis, the standard single-therapy paradigm has failed to meet clinical requirements. Recently, researchers have focused their emphasis on phototherapy and immunogenic cell death (ICD) techniques. In response to the current problems of immunotherapy, a multifunctional drug delivery nanosystem (PDA-IMQ@$CaCO_3$-blinatumomab, PICB) was constructed by using high physiological compatibility of polydopamine (PDA) and calcium carbonate ($CaCO_3$). Toll-like receptor 7 (TLR7) agonist imiquimod (IMQ) and bispecific antibody (BsAb) blinatumomab were loaded onto PDA-$CaCO_3$ nanoparticles (NPs). The findings revealed that the system exhibited the advantages of good dispersion, high stability, excellent physiological compatibility, low toxicity, and high drug loading rate. Compared to the control group, it resulted in a 2.4-fold decrease in $FOXP3^+$ regulatory T-cells within the tumor and a 5.0-fold increase in $CD4^+$ effector T-cells, and promoted the production of damage-related molecular patterns to reinvigorate the ICD effect. PICB had a strong inhibitory effect on tumor growth in 4T1 tumor-bearing mice, and has no toxicity to other organs. Therefore, the multifunctional drug delivery nanosystem constructed in this study could effectively exert the properties of various components *in vivo*, fully demonstrate the synergistic effect between immunotherapy and photothermal therapy, thus significantly improving the tumor therapeutic efficacy, and has a promising clinical application.

1. Introduction

Nowadays, the rising incidence and mortality rates of cancer have posed a significant danger to human health and life [1]. Limited to tumor recurrence and metastasis, the application of single-mode therapies, such as chemotherapy, radiotherapy, and emerging phototherapy, in clinical medicine still has many deficiencies [2]. Immunotherapy is a treatment technique that harnesses the uniqueness of the human immune system to bolster the natural defense against tumor cells. It has become one of the most popular treatment methods in cancer treatment [3]. Targeted killing of tumor stem cells by T-cells mediated by BsAb is a very promising tumor therapy [4,5]. Over the past 30 years, numerous BsAb have been developed, the most common of which is bispecific T-cell engager

* Corresponding author.
** Corresponding author.
E-mail addresses: liuhailong@njnu.edu.cn (H. Liu), zhoujiahong@njnu.edu.cn (J. Zhou).

https://doi.org/10.1016/j.heliyon.2024.e33837
Received 18 April 2024; Received in revised form 27 June 2024; Accepted 27 June 2024
Available online 28 June 2024

(BiTE), which uses a single-chain antibody fragment (scFv) structure. BiTE has been developed for different cancer lines, such as leukemia [6], pancreatic cancer [7], brain cancer [8], and skin cancer [9]. Moreover, in 2014, the Food and Drug Administration (FDA) approved the first BiTE antibody, blinatumomab, for treating leukemia, suggesting that BiTE therapy is indeed a promising approach for treating tumors. Using BiTE-redirected T-cells requires overcoming challenges such as T-cell failure driven by upregulated PD-1 or PD-L1 immune checkpoint proteins, immune escape from tumors, and toxicity to normal tissues [10]. Therefore, BiTE needs to optimize the selection of target tumor-associated antigens (TAAs), adjust its molecular structure, optimize the administration mode, increase the half-life *in vivo*, and implement other improvement programs.

Photothermal therapy can be controlled to occur only at the tumor site, is simple to operate, and is noninvasive, thus minimizing side effects on normal cells [11,12]. PDA has excellent application value in PTT due to its multitudinous functional groups, adhesive properties, efficient photothermal conversion, and biocompatibility [13]. In addition, PDA is easily combined with other nanomaterials when used for drug loading and surface modification, including calcium carbonate ($CaCO_3$) [14,15], iron oxide nanoparticles [16], and gold nanoparticles [17]. Under near-infrared (NIR) irradiation, a photothermal agent absorbs light and produces local hyperthermia, ablating the tumor or inducing tumor apoptosis [18,19]. Unlike normal apoptosis, abnormal cell death and ICD were triggered by chemotherapy drugs such as doxorubicin (DOX), oxaliplatin (OXA), and paclitaxel [20]. PTT-based thermotherapy can also induce the ICD effect and promote the body's immune response to eliminate cancers [21,22]. However, the immune effect triggered by phototherapy is usually weak and cannot form effective immune and antitumor effects. Thus, combining it with other treatments to form enhanced immune and antitumor effects is necessary [23–25].

Therefore, we present a multifunctional nanosystem with both PTT and ICD effects and BiTE based on immunotherapy and phototherapy PDA-IMQ@$CaCO_3$-blinatumomab, PICB for short. In PICB NPs, PDA can be utilized for photothermal treatment of tumor by increasing local temperature under light [26,27]. IMQ, the TLR7 agonist, is a classic clinical drug for the topical treatment of skin cancer [28,29]. Moreover, it is loaded with another biomimetic and mineralized material, $CaCO_3$, an appealing candidate material for bio-applications owing to its excellent biocompatibility [30,31]. More importantly, blinatumomab, a BiTE antibody, developed a specific way to eliminate tumor immunosuppression and restore the ICD effect caused by phototherapy, thus promoting cancer immunotherapy. This system inhibited the activity of regulatory T-cells (Tregs), increased the infiltration of $CD4^+$/$CD8^+$ and IFN-γ^+ cytotoxic T lymphocytes, enhanced the secretion of cytokine IFN-γ, induced more robust T-cell activation, and formed a durable antitumor response. The nanosystem has demonstrated the efficacy of treating cancer using the cascading function (Graphical Abstract): (I) BiTE antibody (blinatumomab) and IMQ suppress Tregs, further abrogating tumor immune suppression and inducing more robust T-cell activation for a durable antitumor response. (II) Synchronously, calcium ions produced by the disintegration of the system can participate in other calcium ion pathways in the body. (III) Meanwhile, with NIR irradiation, thermal ablation of PDA can kill cancer cells directly. When our unique Treg suppression technique is paired with phototherapy, immune suppression is reduced, and the ICD impact is improved, not only eliminating the primary cancer directly but also improving the long-term immune response.

2. Methods

2.1. Synthesis of PICB NPs

The synthesis of PICB NPs consists of four steps. Synthesized PDA-IMQ@$CaCO_3$ NPs according to our laboratory synthesis process in steps 1, 2, and 3 [32–34]. In step 4, PDA-IMQ@$CaCO_3$ NPs aqueous solution (10 mL) and blinatumomab (2 mg) were mixed for 2 h. Then, PDA-IMQ@$CaCO_3$-blinatumomab NPs were obtained.

2.2. In vitro release of IMQ

The release of IMQ from PICB NPs was assessed using the dialysis method. PICB NPs (2.0 mg) were dispersed in PBS (pH 7.4 and pH 5.0, 2 mL) and packaged into dialysis bags (MWCO = 14000 Da). The dialysis bags were immersed in PBS (37 °C, 10 mL) at pH 7.4 and pH 5.0, respectively. The solution (0.5 mL) was collected at 0.5, 1, 2, 4, 6, 8, 10, 12, 24, 36, 48, 60, and 72 h, and the same volume analyzed using of fresh PBS (pH 7.4 and pH 5.0) was added. Finally, the collected solution was analyzed using a UV–vis spectrophotometer at the absorbance of 318 nm.

2.3. In vitro release of Ca^{2+}

The pH response calcium ion release kit was purchased from Beyotime (Shanghai, China). The Ca^{2+} concentration is determined by measuring the absorption value at 575 nm. The standard curve of Ca^{2+} absorbance-concentration was established according to the following equation:

$y = 4.9931x + 0.2221$ ($R^2 = 0.995$).

2.4. Hemolysis

PICB NPs of different concentrations were incubated with 2 % mouse red blood cell saline solution in a 1.5 mL centrifuge tube for 2

h at room temperature. Then, photographs were taken. Subsequently, absorbance (OD value) at 540 nm of samples of each group was detected using an enzyme labeler. The hemolysis rate was calculated according to the following formula:

Hemolysis rate = $(OD_{experimenta}\text{-}OD_{negative\ control})/\ (OD_{positive\ control}\text{-}OD_{negative\ control})$.

2.5. Cell endocytosis

4T1 cells were inoculated in a six-well plate (3×10^5 cells/well) and cocultured with PICB NPs for 2, 4, 12, and 24 h. Then, the cells were rinsed three times with PBS, fixed with 4 % paraformaldehyde, and finally observed under a microscope.

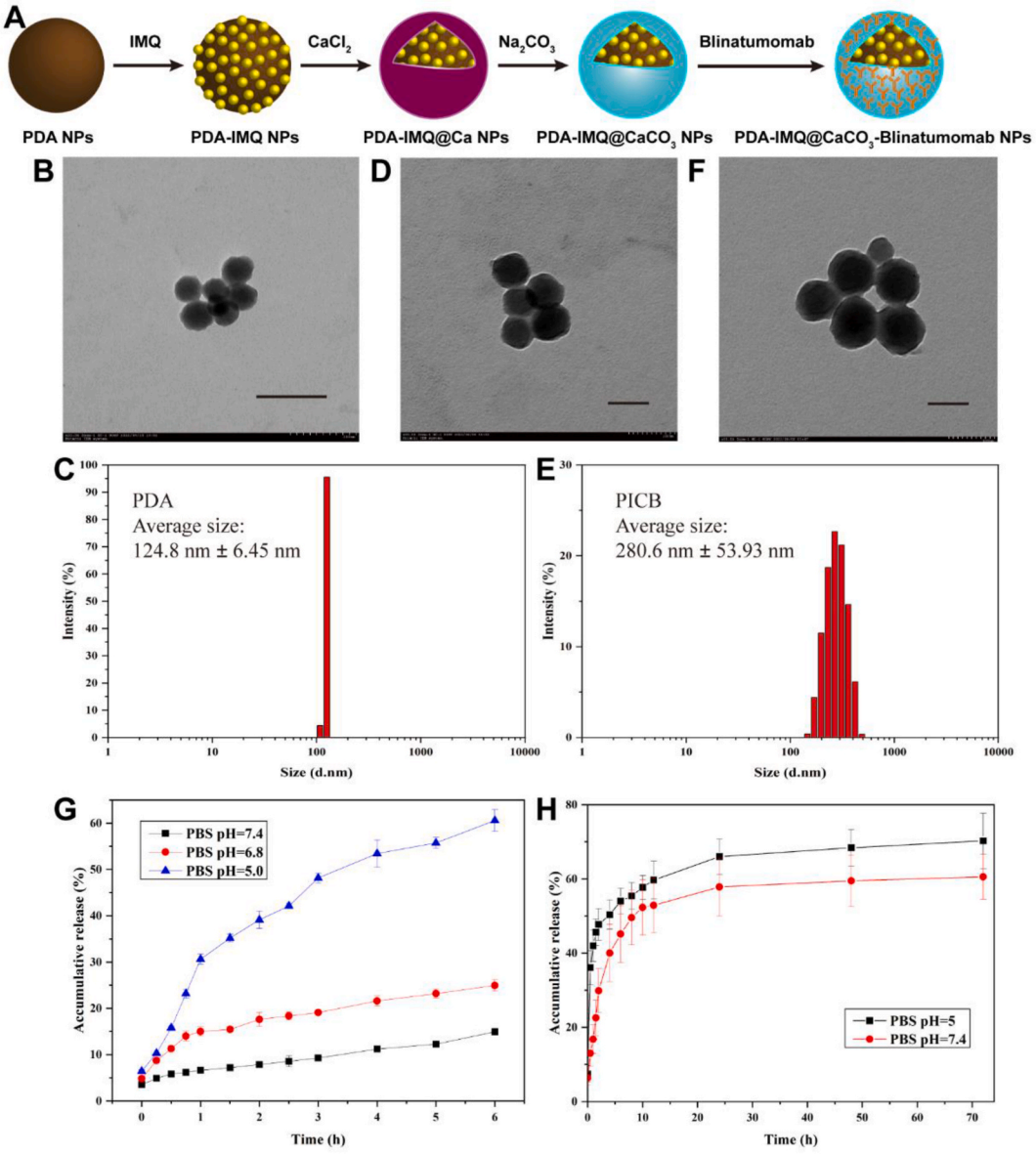

Fig. 1. Characterization data of PICB NPs.
(A) Fabrication of the process of PICB NPs. (B) The TEM images of PDA and (D) PICB NPs immediately (Scale bar: 200 nm). (C, E) DLS determination of PDA and PICB NPs. (F) TEM images of PICB NPs after 30 days. Scale bar: 200 nm. (G) Ca^{2+} cumulative release curves of PICB NPs in PBS (pH 7.4, pH 6.5 and pH 5.0) at 37 °C. (H) IMQ release profiles from PICB NPs in PBS (pH 7.4 and pH 5.0) at 37 °C.

2.6. In vivo tumor studies

For photothermal immunotherapy, when the tumors grew to 5–6 mm in diameter, the mice were randomly divided into five groups (n = 5 per group), namely PBS treated, PDA with NIR laser treated, PDA-IMQ with NIR laser treated, PDA-IMQ@$CaCO_3$ with NIR laser treated, and PICB NPs with NIR laser treated. Mice were tail-intravenously inoculated with NPs (the dose of each component is PDA: 200 μg/mouse, IMQ: 60 μg/mouse, and blinatumomab: 20 μg/mouse). The tumor size was calculated using the following formula: (length × width × height)/2. After 10 days, mice were euthanized, the blood was collected, and the major organs were isolated and fixed in 10 % formalin, followed by staining with hematoxylin and eosin (H&E).

3. Results

3.1. Synthesis and characterization of PICB NPs

A mixture of methanol, water, and Tris was used for the synthesis of PDA NPs using dopamine as the primary raw material [33,34]. IMQ can be anchored to PDA by electrostatics and/or hydrogen bonds. Then, the particles were covered with a $CaCO_3$ shell. Subsequently, blinatumomab was coated onto the surface of PDA-IMQ@$CaCO_3$ NPs primarily through electrostatic adsorption (Fig. 1A). The average dynamic light scattering (DLS) of PDA was approximately 124.8 ± 6.45 nm (Fig. 1B and C) with zeta potential of −25.74 mV. After integrating IMQ, $CaCO_3$, and blinatumomab, the average DLS of PICB NPs was increased to around 280.6 ± 53.93 nm (Fig. 1D and E), whereas the zeta potential remained negative with no significant change (Fig. S1A). TEM images and average DLS in water and FBS visually demonstrated that the particle shape and size of PICB NPs remained unchanged after 30 days at 4 °C (Fig. 1F and S1B). Furthermore, in the presence of hydrogen peroxide, PDA NPs started degrading after 24 h, which was conducive to its metabolism *in vivo* [33]. Additionally, Fourier transform infrared (FTIR) spectroscopy also exhibited the successful construction of PICB NPs (Fig. S1C). A large and broad absorption peaks in the range of 3600 to 3200 cm^{-1} was observed in the synthesized nanoparticles, indicating the presence of hydroxyl and amino groups in the structure. The absence of stretching vibration peaks in N–H, compared to infrared absorption peaks in PDA NPs, suggests effective drug delivery. The characteristic absorption bands of $CaCO_3$ that appeared at

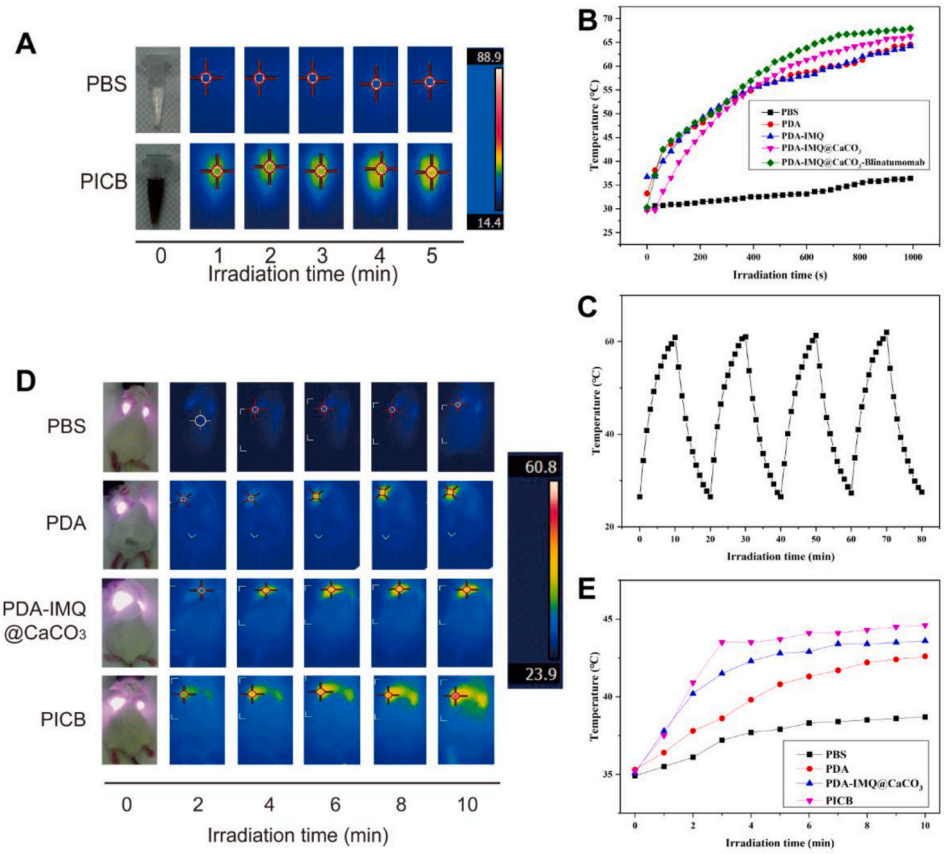

Fig. 2. The photothermal effect of PICB NPs *in vitro* and *in vivo*.
(A) NIR thermal image and (B) heating curve under 808 nm laser at 1.0 W cm^{-2}. (C) Photothermal conversion curve of PICB for four cycles light irradiation. (D) NIR thermal image of 4T1 tumor-bearing mice and (E) temperature changing curves for different time points.

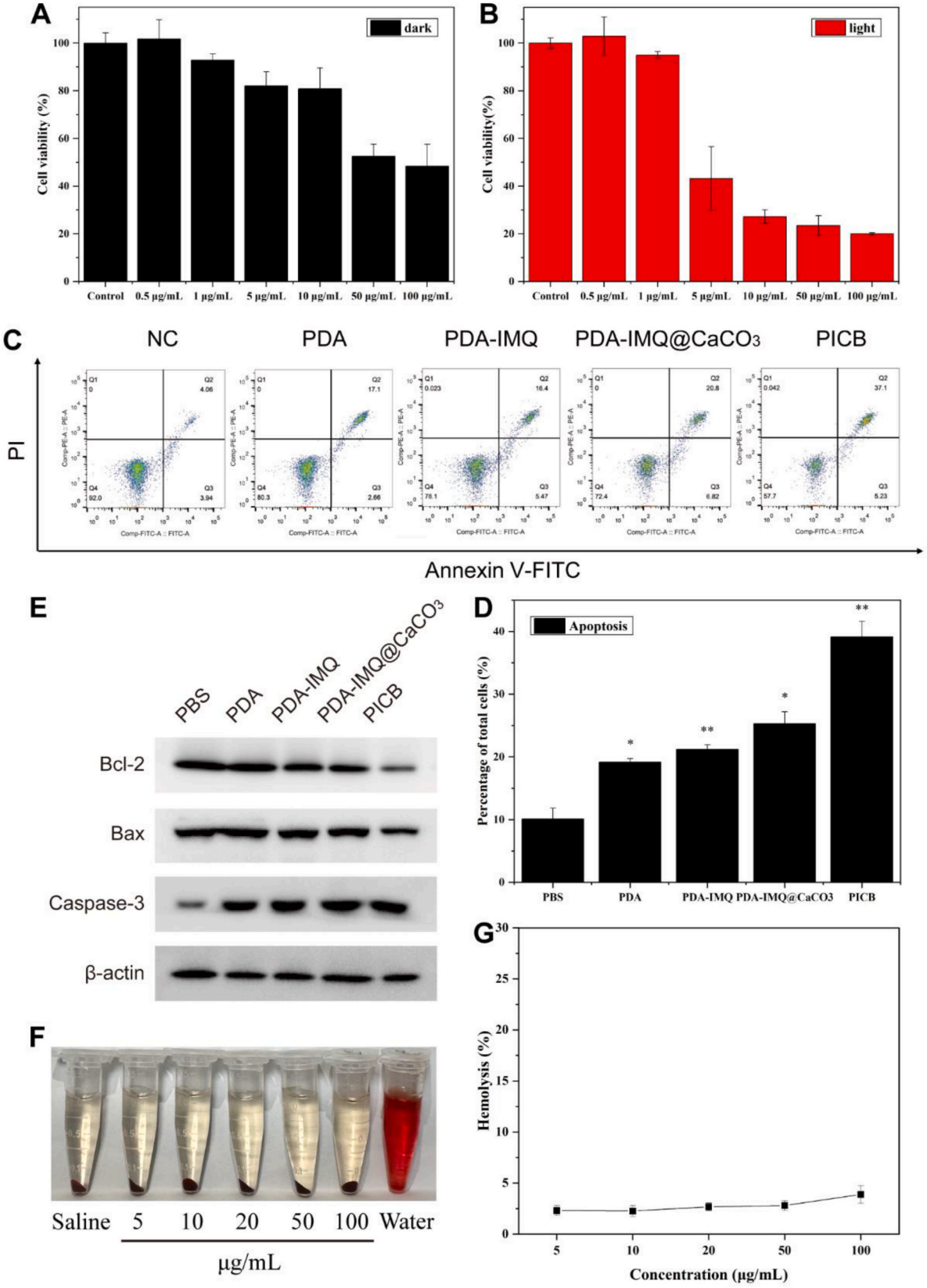

(caption on next page)

Fig. 3. Cellular therapeutic effects of the PICB NPs *in vitro*.
(A, B) Relative viabilities of 4T1 treated with various PICB NPs concentrations without or with laser irradiation. (C) Cellular apoptosis and (D) the analysis with laser irradiation for 24 h. (E) Analysis of apoptosis-related proteins by polyacrylamide gel electrophoresis. (F) Hemolysis photos with different concentrations of PICB NPs. (G) Hemolysis rate of different concentrations of PICB NPs. *P < 0.05, **P < 0.01. ***P < 0.001.

875 cm^{-1} were attributed to the existence of carbonate ions.

$CaCO_3$ is a natural pH reactive biological mineral, basically stable at a pH of 7.4 in aqueous solution conditions and easily decomposed into Ca^{2+} and CO_2 under acidic conditions [35–37]. Prior studies revealed that in the acidic tumor microenvironment, $CaCO_3$-based nanocarriers would be broken down, releasing coated chemotherapy drugs and Ca^{2+} [38]. The explosive release of Ca^{2+} in cancer cells can induce cancer cell death by disrupting Ca^{2+} homeostasis, impairing mitochondrial function, and boosting intracellular ROS levels [39]. Based on the above advantages, $CaCO_3$ is very reliable as a capping material for encapsulating bioactive molecules before the nanocarriers reach the target lesion site while releasing therapeutic drugs in the acidic tumor microenvironment. In PICB NPs, the calcium ion content is about 28.15 % (wt%). Simulating different environments of blood circulation (pH 7.4), peritumor (pH 6.8), and endoplasmic/lysosome (pH 5.0), the *in vitro* Ca^{2+} release of PICB NPs at different pH values is displayed at the left of Fig. 1G. At pH 7.4, the dissolution of NPs is very slow, and only 10 % is released after 6 h. Moreover, at pH 6.8, Ca^{2+} was released slightly faster and about 20 % was released at the end of the experiment. Conversely, the release of NPs at 6 h at pH 5.0 was nearly 60 %, which was three times and six times of that at pH 6.8 and pH 7.4, respectively. Additionally, there was a sudden release of Ca^{2+} in the first 1 h, followed by a plateau until the end of release. These results indicate that the Ca^{2+} release of PICB NPs is highly sensitive to pH, and there is almost no Ca^{2+} release at pH 7.4, ensuring the safety of PICB NPs in the blood circulation, whereas Ca^{2+} release at pH 5.0 can achieve localized release of drugs in the lysosome. It can also be used to induce blood clotting in tumor vessels to treat tumor starvation.

The loading capacity of IMQ in PICB NPs was measured to be 10 %, and the loading efficiency of IMQ in PICB NPs was measured to reach 29 %. The loading efficiency of blinatumomab in PICB NPs was calculated to be 27.03 % using the BCA method, and the loading efficiency was about 54 %. UV–vis–NIR spectra (Fig. S1D) exhibited that PICB NPs possessed the typical absorption peak of IMQ, PDA, and blinatumomab. Fig. 1H depicts the *in vitro* IMQ release of PICB NPs at various pH values, imitating different settings such as blood circulation (pH 7.4) and lysosomes (pH 5.0). IMQ suddenly released in the first 1 h, with around 50 % released, followed by a plateau until the end of the release, which reached about 70 %. At pH 7.4, the release of IMQ was very slow, reaching only 50 % after 10 h. There was almost no drug release after 10 h. In contrast, IMQ showed sustained release under pH 5.0, with drug release for 48 h.

3.2. Photothermal effect of PICB NPs in vitro and in vivo

The photothermal effect was investigated by monitoring the temperature of PBS, PDA, PDA-IMQ, PDA-IMQ@$CaCO_3$, and PICB NPs after irradiation by NIR laser (808 nm, 1 W cm^{-2}). The temperature of PICB NPs aqueous solution was measured, the results showed that it gradually increased to about 57 °C within 10 min and remained stable in about 15 min (Fig. 2A). At the same concentration, the temperature of PICB NPs solution increased to 67.9, exhibiting good photothermal properties *in vitro* (Fig. 2A). Moreover, Fig. 2B illustrates exhibited the photothermal capability of PICB NPs. Additionally, after four irradiation cycles by a laser (808 nm, 1 W cm^{-2}, 10 min for each cycle), the heating curve (Fig. 2C) of PICB NPs seemed unchanged, indicating good photostability. PDA NPs can effectively absorb NIR irradiation, and their photothermal conversion efficiency is as high as 40 % [17,33,40–42]. The photothermal conversion efficiency of PICB NPs under 1 W cm^{-2} was measured to be 72.93 % (Figs. S2A–B), higher than other nanoparticles with PDA and $CaCO_3$ as shells and cores alone [14,15].

Subsequently, their photothermal properties in tumor-bearing mice were studied. The tumor of the PDA NPs, PICB NPs or saline-treated mice was irradiated using an 808 nm laser (0.3 W cm^{-2}, 10 min). An infrared thermal imager recorded the temperature of the tumor site after NIR. In Fig. 2D and E, no significant temperature change was observed after laser irradiation in control mice. Conversely, the temperature of the tumor site increased significantly in the PDA NPs- and PICB NPs-treated groups. Both *in vivo* and *in vitro* data confirmed the effective photothermal properties of PICB, and guaranteed that their PTT activity can effectively ablate tumor cells.

3.3. Cytotoxicity and cell apoptosis

Fig. S3 demonstrates that PICB NPs are rapidly engulfed by 4T1 cells, with the highest phagocytosis within 4 h and then stabilizing within 24 h. High phagocytosis ensures high cell accumulation of PICB NPs. The control group exhibited intact and smooth 4T1 cell structures. As the duration of the culture rises and the cells continue to preserve their structural integrity, an increasing number of NPs will adhere to and be internalized by the cells. When the cells were irradiated with an 808 nm laser, the high cell accumulation of NPs was more effective in inducing apoptosis. An Annexin V-FITC/PI apoptosis detection kit and MTT assay method were applied to investigate the photocytotoxicity of PICB NPs. Without the use of NIR laser irradiation, PICB NPs demonstrated a 50 % efficacy in killing 4T1 cells (Fig. 3A). Nevertheless, the PICB NPs effectively eliminated approximately 80 % of the cells when exposed to NIR laser irradiation (Fig. 3B), indicating the heightened efficacy of the nanosystem.

According to flow cytometry data (Fig. 3C), PICB NPs induced around 37 % apoptosis after NIR irradiation, and the number of apoptotic cells was about six times more than that in the control group (Fig. 3D). The results of the MTT and apoptosis experiment confirmed each other, indicating that PICB NPs primarily induced apoptosis pathway leading to cell death. To further determine the

apoptosis effect of PICB NPs in cells, we used western blotting (WB) to detect apoptosis-related protein expression in 4T1 cells. Fig. 3E demonstrates that after the addition of the system, the expression levels of Caspase-3 and Bax/Bcl-2 in cells were significantly increased. The PICB NPs exhibited a stronger upregulation trend, suggesting a congenerous effect between IMQ and blinatumomab. The WB data indicated that PICB NPs have a more significant impact on cell apoptosis.

Hemolysis refers to the phenomenon of the cell membrane of red blood cells being broken due to various factors, resulting in the overflow of hemoglobin in the cell. Obviously, a safe drug must avoid inducing red blood cell rupture; otherwise, the drug will cause significant adverse effects and may endanger life owing to hemolysis during transit. Therefore, we investigated the hemolysis of PICB NPs. Normal saline was used as the negative control and ultrapure water was used as the positive control. The hemolysis experiment was conducted with different concentrations of PICB NPs and a normal saline solution. In Fig. 3F, no prominent hemolysis occurred when the concentration of the particles reached 100 μg/mL (hemolysis was evident in the ultrapure water positive control group). Moreover, in Fig. 3G quantitative analysis to detect OD540 revealed that the hemolysis rate in all groups was lower than 5 %, indicating that the nano diagnostic agent had no apparent damage to the erythrocyte membrane.

3.4. *In vivo* anticancer efficacy

The above excellent photothermal properties and *in vitro* therapeutic effect prompted us to investigate the efficacy of PICB NPs *in vivo* immune and photo-combined therapy. The phototherapy effects of PICB NPs were evaluated by randomly dividing 4T1 tumor-bearing mice into five groups (n = 5): (1) control, (2) PDA, (3) PDA-IMQ, (4) PDA-IMQ@$CaCO_3$, and (5) PICB NPs. On days 1, 3,

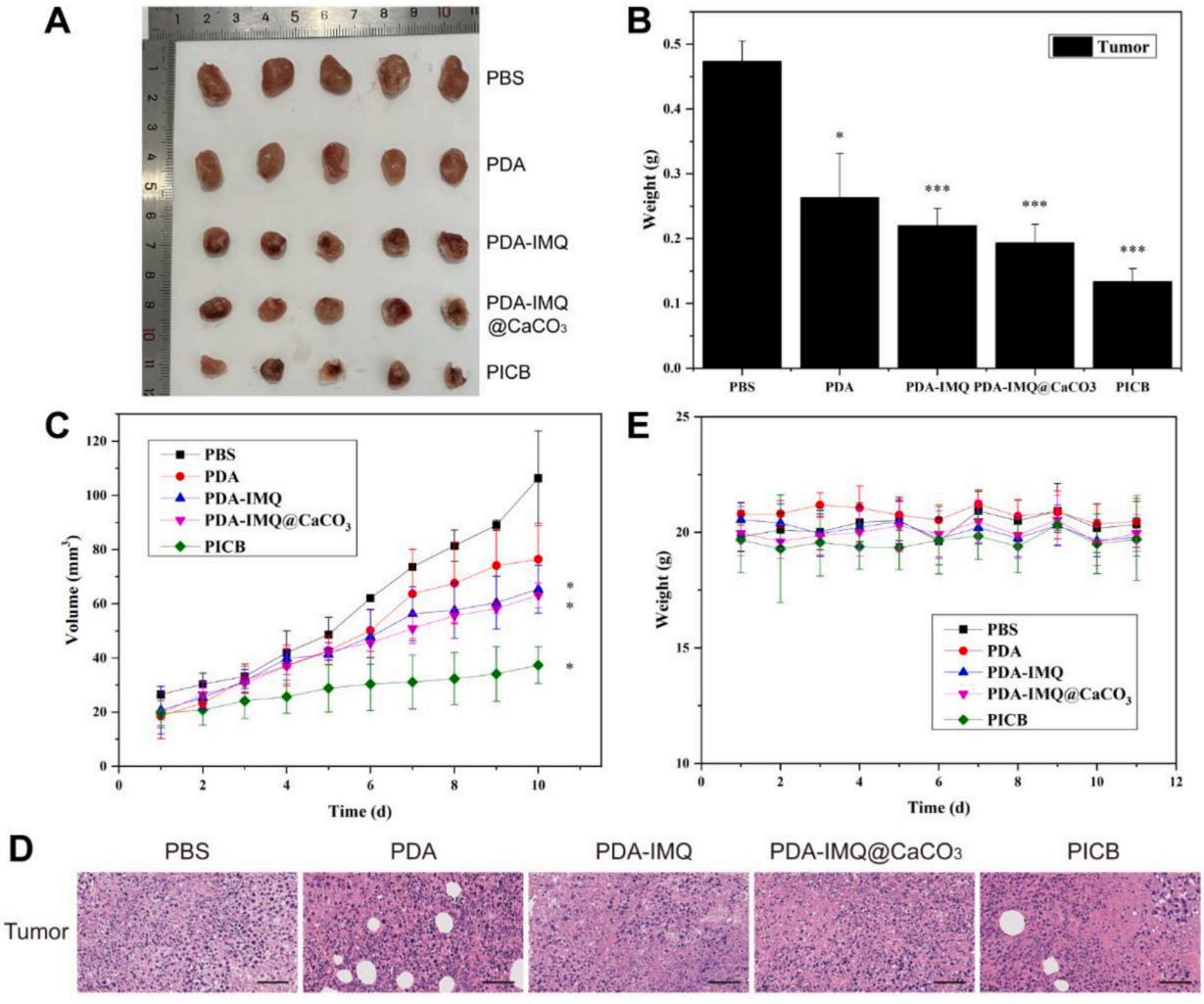

Fig. 4. *In vivo* evaluation of the efficacy of PICB NPs.
(A) Photographs of tumors after treatment in different groups. (B, C) Tumor weight and volume records after treatment in different formulations. (D) H&E staining of paraffin sections of mouse tumors in each group (Scale bar: 100 μm). (E) Weight of tumor-bearing mice during treatment. *P < 0.05, **P < 0.01, ***P < 0.001.

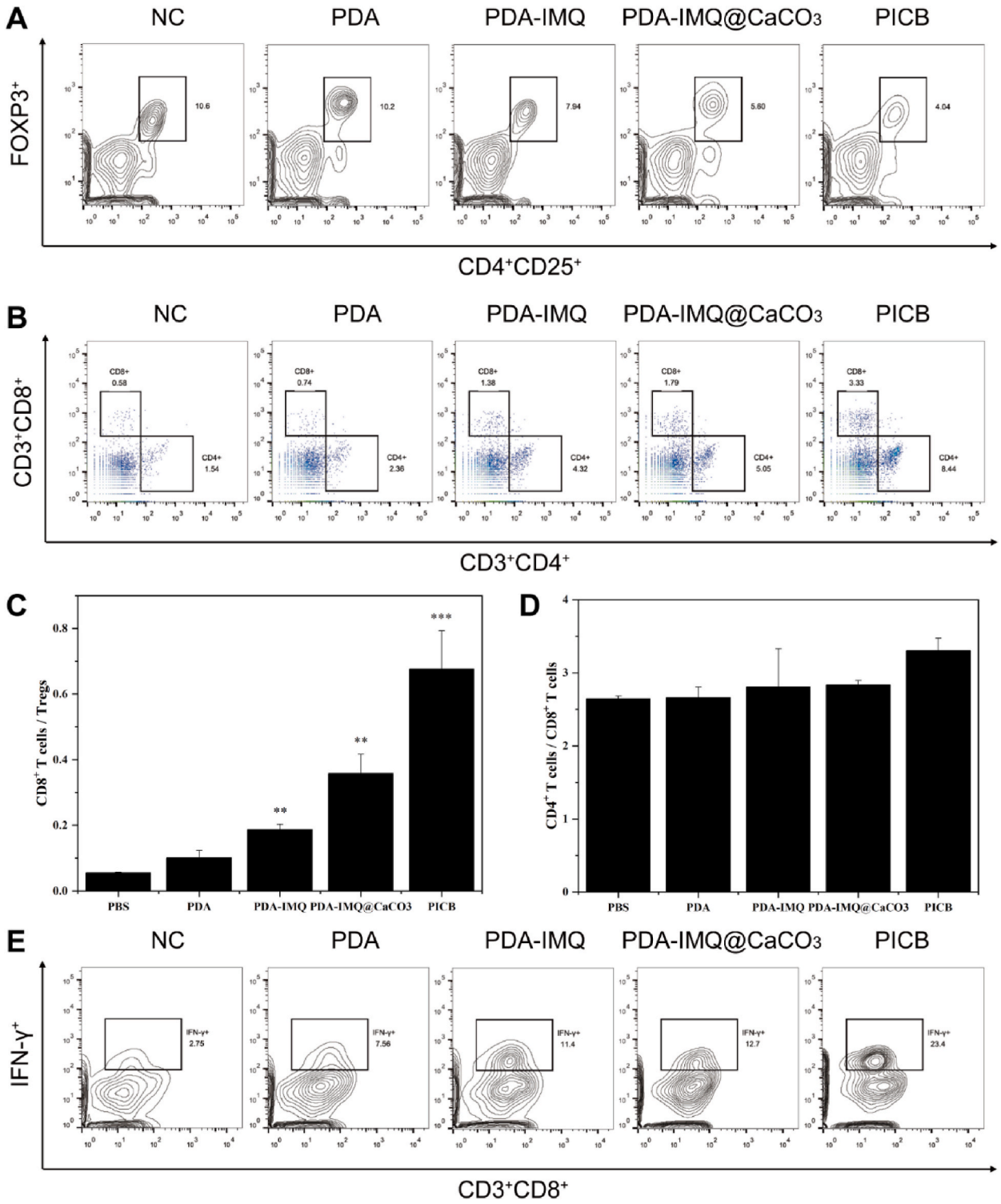

Fig. 5. Suppression of Tregs and activation of T cells *in vivo*.
(A) The proportion of $CD4^+CD25^+FOXP3^+$ Tregs in the spleen of tumor-bearing mice. (gated by $CD3^+CD4^+CD25^+$ cells). (B) The ratio of $CD4^+$ T-cells and $CD8^+$ T-cells in spleens. (gated by $CD3^+$ cells) (C, D) The quantity ratio of $CD8^+$ T lymphocytes/Tregs and $CD4^+$ T lymphocytes/$CD8^+$ T lymphocytes in spleens. (E) Average area of $CD8^+IFN\text{-}\gamma^+$ T lymphocytes in spleens. (gated by $CD3^+CD8^+$ cells) *P < 0.05, **P < 0.01. ***P < 0.001.

5, 7, and 9, drugs were i.v. injected into mice. Expect for groups 1, the other groups were treated with light irradiation 24 h after injection (808 nm, 0.3 W cm^{-2}, 10 min). The tumors were clearly ablated with black scars during therapy with the optimal formulation (Fig. 4A). Based on the tumor weight (Fig. 4B) and growth curve (Fig. 4C), we found that following the combination of PTT with the IMQ and blinatumomab treatment, regression was observed in the tumor beyond effective PTT. PICB NPs *in vivo* could work better than apoptosis *in vitro* (Fig. 3C), which may be associated with the degradation of calcium carbonate and subsequent carbon dioxide formation. H&E staining results of tumor tissues (Fig. 4D) revealed that tumor tissues suffered considerable damage, which certified that PICB NPs had a significant damage effect. This indicates that the introduction of IMQ and blinatumomab during PTT can suppress the growth of the tumor thickness beyond effective PTT and enhance the therapeutic outcome of PTT.

After treatment, photos of the mice's immune organs, the spleen and liver, visually showed the effects of the drug on the immune system (Fig. S4A). The weight of body (Fig. 4E), weight of organs (Figs. S4B–F), and a comparison of major organs from mice stained with H&E revealed that none of the treatments exhibited significant toxicities, but lung tissue sections showed some lung metastases. The above results suggested the hypotoxicity and good biocompatibility of PICB NPs after systematic administration for mice.

3.5. Abrogating tumor immune suppression

We used flow fluorescence antibodies to detect the immunophenotype of immune cells in tumor-bearing mice and explore the immune functions of PICB NPs. Lymphocytes from mouse spleens were isolated at the end of the experiment. In Fig. 5A and Fig. S5A, compared with the control group, PICB NPs notably decreased $CD4^+CD25^+FOXP3^+$ Tregs by 2.4-fold. Besides, in the PICB NP group, the FOXP3 was notable decrease in blood (Fig. S5B).

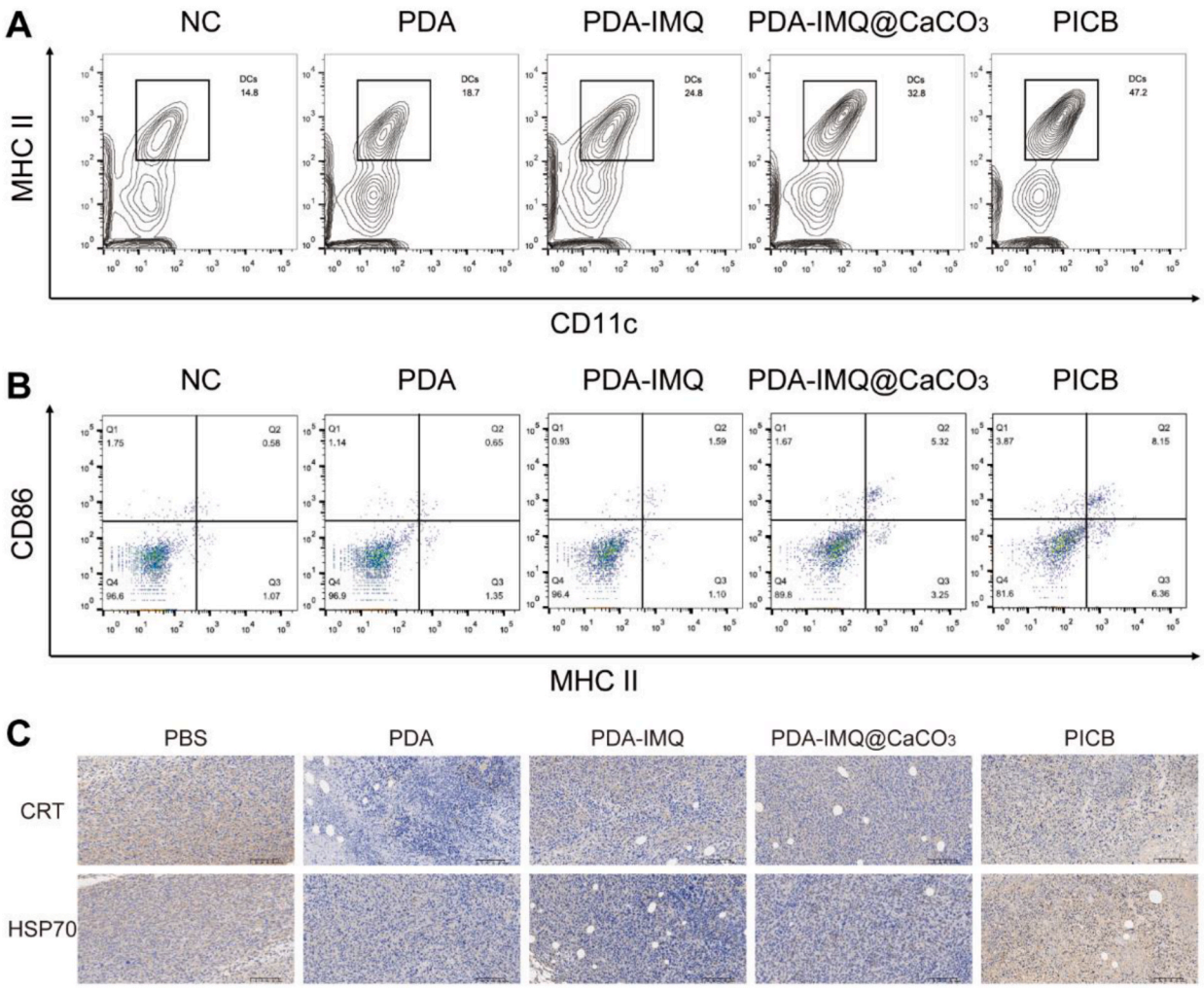

Fig. 6. PICB NPs reactivates ICD.
(A, B) The centage of $CD11c^+MHCII^+$ cells and $MHCII^+CD86^+$ cells in spleens. (gated by $CD11c^+$ cells) (C) IHC staining of CRT and HSP70 in tumor tissues, respectively. Scale bar: 100 μm*P < 0.05, **P < 0.01. ***P < 0.001.

Both $CD4^+$ and $CD8^+$ T lymphocytes play a crucial role in anti-cancer immune response. Therefore, the infiltration of $CD4^+$ and $CD8^+$ T-cells in the spleen of mice was evaluated (Fig. 5B). Compared with the control group, there was a significant quantity of growth in $CD8^+$ T lymphocytes and $CD4^+$ T lymphocytes in the PICB NPs treatment group (5.7-fold) (Figs. S5C–D). The ratios of $CD8^+$ T lymphocytes/Tregs and $CD4^+$ T lymphocytes/$CD8^+$ T lymphocytes in the PICB NPs treatment group were slightly increased compared with those in other groups (Fig. 5C and D). These findings indicated that PICB NPs containing BiTE antibody (blinatumomab) could restrain Tregs. Consequently, cancer therapies can achieve much more effective immune responses.

The immunoregulatory and antitumor properties of IFN-γ make it useful for cancer treatment [43]. For further evaluation the immune activation capacity of the PICB NPs, the ratio of $CD8^+$IFN-γ^+ T lymphocytes in mice's spleens was examined (Fig. 5E). $CD8^+$IFN-γ^+ T lymphocytes in PICB NPs-treated mice were significantly greater than those in nontreated mice (Fig. S5E). The drug delivery system increased its IFN-γ levels in the blood, contributing to induced antitumor immunity using PICB NPs (Fig. S5F).

3.6. Reinvigoration of ICD

APC-mediated T-cell activation was simulated with bone marrow dendritic cells (BMDCs) [44]. During ICD, DAMPs are released, and receptors expressed on DCs are activated [45]. All phototherapy-treated group, especially PICB NPs-treated group, exhibited an increased MHCII expression (Fig. 6A). Moreover, compared to the control group, the maturation of DCs treated by PICB NPs was enhanced obviously (Fig. S6A), as indicated by the increased expressions of $CD11c^+MHCII^+$ and $MHCII^+CD86^+$(Fig. 6B and S6B), elucidating that PICB NPs could promote the *in vivo* DCs maturation.

Subsequently, immunohistochemical (IHC) analyses were conducted to detect ICD reactivation (Fig. 6C). The data demonstrated that calreticulin (CRT) exposure and HSP70 secretion in paraffin sections of tumor of tumor-bearing mice were decreased when PDA alone compared with those in the control group, and significantly increased when PICB was used (Figs. S6C–D). The findings stated that PICB NPs combining BiTE with phototherapy induced APC activation for the ICD effect, leading to enhanced immunotherapy for cancer.

4. Conclusion

By inhibiting Tregs and reinvigorating the ICD effect, the nanosystem's phototherapy and BiTE activities stimulate effective immunity. Based on these findings, PICB NPs offer a wide range of potential applications for enhancing cancer treatment. The system combines photothermal therapy and immunotherapy to target tumor areas and drug delivery. Irradiated with a NIR laser, IMQ and blinatumomab can be released from PICB NPs and specifically kill tumor cells and enhance immune response by recruiting immune cells and inhibiting ICD effect. These findings indicate that the nanosystem built not only renders the loaded medications fully effective but also enhances efficacy through the synergistic effect of the two therapies. The construction concept has a unique benefit in promoting the clinical application of drug delivery nanosystems.

Funding

This work was supported by the 2021 Jiangsu Province biomedical materials testing service platform, Jiangsu Province, China.

Data availability statement

No data associated with this study has been deposited into a publicly available repository. The authors do not have permission to share data.

Ethics statement

The goal of the current study was to eliminate tumors by stimulating the body's immune system. There are no substitutes for mimicking the immune system at the moment because of its complexity. The most efficient and necessary method in this investigation to confirm the therapeutic effect of the drug delivery nanosystem on tumor immunity is therefore animal model validation. In our study, 50 4∼6-week BALB/c mice were supplied by the Qinglong Mountain (Jiangsu, China) and carefully housed in the laboratory animal center of Nanjing Normal university (Jiangsu, China) under constant temperature and humidity. All mice were utilized *in vivo* experiments after being given isoflurane anesthesia. The whole procedures were conducted in accordance with the National Institutes of Health Guide for the Care and Use of Laboratory Animals, and with the guidelines for the care and use of animals established by the Animal Care and Use Committee of Nanjing Normal University (IACUC-20220101), and at the conclusion of the study, all mice were decollated and put to death. All animal experiments were performed following the ARRIVE guidelines.

CRediT authorship contribution statement

RuYan Li: Writing – original draft, Methodology, Data curation. **XianDong Shi:** Validation, Methodology. **JingYi Zhang:** Validation, Methodology. **BaoQing Liu:** Validation, Methodology. **Jian Shen:** Writing – review & editing, Data curation. **HaiLong Liu:** Writing – review & editing, Data curation. **JiaHong Zhou:** Writing – review & editing, Funding acquisition, Data curation.

Declaration of competing Interest

The authors declare that they have no known competing financial interests or personal relationships that could have appeared to influence the work reported in this paper.

Appendix A. Supplementary data

Supplementary data to this article can be found online at https://doi.org/10.1016/j.heliyon.2024.e33837.

References

[1] H. Sung, J. Ferlay, R.L. Siegel, M. Laversanne, I. Soerjomataram, A. Jemal, F. Bray, Global cancer statistics 2020: GLOBOCAN estimates of incidence and mortality worldwide for 36 cancers in 185 countries, CA A Cancer J. Clin. 71 (3) (2021) 209–249, https://doi.org/10.3322/caac.21660.

[2] J. Jiang, N. Shen, T. Ci, Z. Tang, Z. Gu, G. Li, X. Chen, Combretastatin A4 nanodrug-induced MMP9 amplification boosts tumor-selective release of doxorubicin prodrug, Adv. Mater. 31 (44) (2019) e1904278, https://doi.org/10.1002/adma.201904278.

[3] I. Mellman, G. Coukos, G. Dranoff, Cancer immunotherapy comes of age, Nature 480 (7378) (2011) 480–489, https://doi.org/10.1038/nature10673.

[4] A. Thakur, L.G. Lum, "NextGen" biologics: bispecific antibodies and emerging clinical results, Expet Opin. Biol. Ther. 16 (5) (2016) 675–688, https://doi.org/10.1517/14712598.2016.1150996.

[5] U. Brinkmann, R.E. Kontermann, Bispecific antibodies, Science 372 (6545) (2021) 916–917, https://doi.org/10.1126/science.abg1209.

[6] R. Bargou, E. Leo, G. Zugmaier, M. Klinger, M. Goebeler, S. Knop, R. Noppeney, A. Viardot, G. Hess, M. Schuler, H. Einsele, C. Brandl, A. Wolf, P. Kirchinger, P. Klappers, M. Schmidt, G. Riethmuller, C. Reinhardt, P.A. Baeuerle, P. Kufer, Tumor regression in cancer patients by very low doses of a T cell-engaging antibody, Science 321 (5891) (2008) 974–977, https://doi.org/10.1126/science.1158545.

[7] M. Cioffi, J. Dorado, P.A. Baeuerle, C. Heeschen, EpCAM/CD3-Bispecific T-cell engaging antibody MT110 eliminates primary human pancreatic cancer stem cells, Clin. Cancer Res. 18 (2) (2012) 465–474, https://doi.org/10.1158/1078-0432.CCR-11-1270.

[8] B.D. Choi, C.T. Kuan, M. Cai, G.E. Archer, D.A. Mitchell, P.C. Gedeon, L. Sanchez-Perez, I. Pastan, D.D. Bigner, J.H. Sampson, Systemic administration of a bispecific antibody targeting EGFRvIII successfully treats intracerebral glioma, Proc. Natl. Acad. Sci. U.S.A. 110 (1) (2013) 270–275, https://doi.org/10.1073/pnas.1219817110.

[9] H. Torisu-Itakura, H.F. Schoellhammer, M.S. Sim, R.F. Irie, S. Hausmann, T. Raum, P.A. Baeuerle, D.L. Morton, Redirected lysis of human melanoma cells by a MCSP/CD3-bispecific BiTE antibody that engages patient-derived T cells, J. Immunother. 34 (8) (2011) 597–605, https://doi.org/10.1097/CJI.0b013e3182307fd8.

[10] M.E. Goebeler, R.C. Bargou, T cell-engaging therapies - BiTEs and beyond, Nat. Rev. Clin. Oncol. 17 (7) (2020) 418–434, https://doi.org/10.1038/s41571-020-0347-5.

[11] D.E. Dolmans, D. Fukumura, R.K. Jain, Photodynamic therapy for cancer, Nat. Rev. Cancer 3 (5) (2003) 380–387, https://doi.org/10.1038/nrc1071.

[12] Z. Xie, T. Fan, J. An, W. Choi, Y. Duo, Y. Ge, B. Zhang, G. Nie, N. Xie, T. Zheng, Y. Chen, H. Zhang, J.S. Kim, Emerging combination strategies with phototherapy in cancer nanomedicine, Chem. Soc. Rev. 49 (22) (2020) 8065–8087, https://doi.org/10.1039/d0cs00215a.

[13] J. Zhu, Z. Wang, X. Xu, M. Xu, X. Yang, C. Zhang, J. Liu, F. Zhang, X. Shuai, W. Wang, Z. Cao, Polydopamine-Encapsulated perfluorocarbon for ultrasound contrast imaging and photothermal therapy, Mol. Pharm. 17 (3) (2020) 817–826, https://doi.org/10.1021/acs.molpharmaceut.9b01070.

[14] P. Xue, M. Hou, L. Sun, Q. Li, L. Zhang, Z. Xu, Y. Kang, Calcium-carbonate packaging magnetic polydopamine nanoparticles loaded with indocyanine green for near-infrared induced photothermal/photodynamic therapy, Acta Biomater. 81 (2018) 242–255, https://doi.org/10.1016/j.actbio.2018.09.045.

[15] W. Zhong, K.H. Wong, F. Xu, N. Zhao, M. Chen, NIR-responsive polydopamine-based calcium carbonate hybrid nanoparticles delivering artesunate for cancer chemo-photothermal therapy, Acta Biomater. 145 (2022) 135–145, https://doi.org/10.1016/j.actbio.2022.03.051.

[16] X. Zheng, H. Wu, S. Wang, J. Zhao, L. Hu, Preparation and characterization of biocompatible iron/zirconium/polydopamine/carboxymethyl chitosan hydrogel with fenton catalytic properties and photothermal efficacy, Gels 9 (6) (2023), https://doi.org/10.3390/gels9060452.

[17] Y. Liu, Z. Li, Z. Yin, H. Zhang, Y. Gao, G. Huo, A. Wu, L. Zeng, Amplified photoacoustic signal and enhanced photothermal conversion of polydopamine-coated gold nanobipyramids for phototheranostics and synergistic chemotherapy, ACS Appl. Mater. Interfaces 12 (13) (2020) 14866–14875, https://doi.org/10.1021/acsami.9b22979.

[18] S. Ye, J. Rao, S. Qiu, J. Zhao, H. He, Z. Yan, T. Yang, Y. Deng, H. Ke, H. Yang, Y. Zhao, Z. Guo, H. Chen, Rational design of conjugated photosensitizers with controllable photoconversion for dually cooperative phototherapy, Adv. Mater. (2018) e1801216, https://doi.org/10.1002/adma.201801216.

[19] J. Chen, C. Ning, Z. Zhou, P. Yu, Y. Zhu, G. Tan, C. Mao, Nanomaterials as photothermal therapeutic agents, Prog. Mater. Sci. 99 (2019) 1–26, https://doi.org/10.1016/j.pmatsci.2018.07.005.

[20] X. Feng, W. Xu, Z. Li, W. Song, J. Ding, X. Chen, Immunomodulatory nanosystems, Adv. Sci. 6 (17) (2019) 1900101, https://doi.org/10.1002/advs.201900101.

[21] D.V. Krysko, A.D. Garg, A. Kaczmarek, O. Krysko, P. Agostinis, P. Vandenabeele, Immunogenic cell death and DAMPs in cancer therapy, Nat. Rev. Cancer 12 (12) (2012) 860–875, https://doi.org/10.1038/nrc3380.

[22] H. Kobayashi, P.L. Choyke, Near-infrared photoimmunotherapy of cancer, Acc. Chem. Res. 52 (8) (2019) 2332–2339, https://doi.org/10.1021/acs.accounts.9b00273.

[23] X. Duan, C. Chan, N. Guo, W. Han, R.R. Weichselbaum, W. Lin, Photodynamic therapy mediated by nontoxic core-shell nanoparticles synergizes with immune checkpoint blockade to elicit antitumor immunity and antimetastatic effect on breast cancer, J. Am. Chem. Soc. 138 (51) (2016) 16686–16695, https://doi.org/10.1021/jacs.6b09538.

[24] C. He, X. Duan, N. Guo, C. Chan, C. Poon, R.R. Weichselbaum, W. Lin, Core-shell nanoscale coordination polymers combine chemotherapy and photodynamic therapy to potentiate checkpoint blockade cancer immunotherapy, Nat. Commun. 7 (2016) 12499, https://doi.org/10.1038/ncomms12499.

[25] J. Xu, L. Xu, C. Wang, R. Yang, Q. Zhuang, X. Han, Z. Dong, W. Zhu, R. Peng, Z. Liu, Near-infrared-triggered photodynamic therapy with multitasking upconversion nanoparticles in combination with checkpoint blockade for immunotherapy of colorectal cancer, ACS Nano 11 (5) (2017) 4463–4474, https://doi.org/10.1021/acsnano.7b00715.

[26] B. Poinard, S.Z.Y. Neo, E.L.L. Yeo, H.P.S. Heng, K.G. Neoh, J.C.Y. Kah, Polydopamine nanoparticles enhance drug release for combined photodynamic and photothermal therapy, ACS Appl. Mater. Interfaces 10 (25) (2018) 21125–21136, https://doi.org/10.1021/acsami.8b04799.

[27] Y. Liu, K. Ai, J. Liu, M. Deng, Y. He, L. Lu, Dopamine-melanin colloidal nanospheres: an efficient near-infrared photothermal therapeutic agent for in vivo cancer therapy, Adv. Mater. 25 (9) (2013) 1353–1359, https://doi.org/10.1002/adma.201204683.

[28] F. Aranda, E. Vacchelli, F. Obrist, A. Eggermont, J. Galon, C. Sautes-Fridman, I. Cremer, J. Henrik Ter Meulen, L. Zitvogel, G. Kroemer, L. Galluzzi, Trial Watch: toll-like receptor agonists in oncological indications, OncoImmunology 3 (2014) e29179, https://doi.org/10.4161/onci.29179.

[29] T.C.B. Klauber, J.M. Laursen, D. Zucker, S. Brix, S.S. Jensen, T.L. Andresen, Delivery of TLR7 agonist to monocytes and dendritic cells by DCIR targeted liposomes induces robust production of anti-cancer cytokines, Acta Biomater. 53 (2017) 367–377, https://doi.org/10.1016/j.actbio.2017.01.072.

[30] X.W. He, T. Liu, Y.X. Chen, D.J. Cheng, X.R. Li, Y. Xiao, Y.L. Feng, Calcium carbonate nanoparticle delivering vascular endothelial growth factor-C siRNA effectively inhibits lymphangiogenesis and growth of gastric cancer in vivo, Cancer Gene Ther. 15 (3) (2008) 193–202, https://doi.org/10.1038/sj.cgt.7701122.

[31] A. Som, R. Raliya, L. Tian, W. Akers, J.E. Ippolito, S. Singamaneni, P. Biswas, S. Achilefu, Monodispersed calcium carbonate nanoparticles modulate local pH and inhibit tumor growth in vivo, Nanoscale 8 (25) (2016) 12639–12647, https://doi.org/10.1039/c5nr06162h.
[32] Q. Zhan, X. Shi, J. Zhou, L. Zhou, S. Wei, Drug-controlled release based on complementary base pairing rules for photodynamic-photothermal synergistic tumor treatment, Small 15 (3) (2019) e1803926, https://doi.org/10.1002/smll.201803926.
[33] R. Li, Q. Zheng, Q. Deng, Y. Wang, H. Yang, J. Shen, Y. Liu, J. Zhou, A dual functional drug delivery system that combines photothermal therapy and immunotherapy to treat tumors, Mol. Pharm. 19 (5) (2022) 1449–1457, https://doi.org/10.1021/acs.molpharmaceut.1c00999.
[34] R. Li, X. Huang, X. Li, H. Liu, J. Zhou, J. Shen, A multi-functional drug delivery nanosystem release of TLR-7 immunostimulant and OKT3 induced efficient cancer immunotherapy, Photodiagnosis Photodyn. Ther. 44 (2023) 103834, https://doi.org/10.1016/j.pdpdt.2023.103834.
[35] Y. Svenskaya, B. Parakhonskiy, A. Haase, V. Atkin, E. Lukyanets, D. Gorin, R. Antolini, Anticancer drug delivery system based on calcium carbonate particles loaded with a photosensitizer, Biophys. Chem. 182 (2013) 11–15, https://doi.org/10.1016/j.bpc.2013.07.006.
[36] X. Zhao, Z. Yuan, L. Yildirimer, J. Zhao, Z.Y. Lin, Z. Cao, G. Pan, W. Cui, Tumor-triggered controlled drug release from electrospun fibers using inorganic caps for inhibiting cancer relapse, Small 11 (34) (2015) 4284–4291, https://doi.org/10.1002/smll.201500985.
[37] H. Li, Y. Feng, Q. Luo, Z. Li, X. Li, H. Gan, Z. Gu, Q. Gong, K. Luo, Stimuli-activatable nanomedicine meets cancer theranostics, Theranostics 13 (15) (2023) 5386–5417, https://doi.org/10.7150/thno.87854.
[38] Y. Zhao, Z. Luo, M. Li, Q. Qu, X. Ma, S.H. Yu, Y. Zhao, A preloaded amorphous calcium carbonate/doxorubicin@silica nanoreactor for pH-responsive delivery of an anticancer drug, Angew. Chem., Int. Ed. Engl. 54 (3) (2015) 919–922, https://doi.org/10.1002/anie.201408510.
[39] P. Zheng, B. Ding, Z. Jiang, W. Xu, G. Li, J. Ding, X. Chen, Ultrasound-augmented mitochondrial calcium ion overload by calcium nanomodulator to induce immunogenic cell death, Nano Lett. 21 (5) (2021) 2088–2093, https://doi.org/10.1021/acs.nanolett.0c04778.
[40] J. Leng, X. Dai, X. Cheng, H. Zhou, D. Wang, J. Zhao, K. Ma, C. Cui, L. Wang, Z. Guo, Biomimetic cucurbitacin B-polydopamine nanoparticles for synergistic chemo-photothermal therapy of breast cancer, Front. Bioeng. Biotechnol. 10 (2022) 841186, https://doi.org/10.3389/fbioe.2022.841186.
[41] X. Qi, Y. Huang, S. You, Y. Xiang, E. Cai, R. Mao, W. Pan, X. Tong, W. Dong, F. Ye, J. Shen, Engineering robust Ag-decorated polydopamine nano-photothermal platforms to combat bacterial infection and prompt wound healing, Adv. Sci. 9 (11) (2022) e2106015, https://doi.org/10.1002/advs.202106015.
[42] Z. Du, R. Ma, S. Chen, H. Fan, Y. Heng, T. Yan, G. Alimu, L. Zhu, X. Zhang, N. Alifu, C. Ma, A highly efficient polydopamine encapsulated clinical ICG theranostic nanoplatform for enhanced photothermal therapy of cervical cancer, Nanoscale Adv. 4 (18) (2022) 4016–4024, https://doi.org/10.1039/d2na00341d.
[43] M.A. Kursunel, G. Esendagli, The untold story of IFN-gamma in cancer biology, Cytokine Growth Factor Rev. 31 (2016) 73–81, https://doi.org/10.1016/j.cytogfr.2016.07.005.
[44] D. Zhang, T. Wu, X. Qin, Q. Qiao, L. Shang, Q. Song, C. Yang, Z. Zhang, Intracellularly generated immunological gold nanoparticles for combinatorial photothermal therapy and immunotherapy against tumor, Nano Lett. 19 (9) (2019) 6635–6646, https://doi.org/10.1021/acs.nanolett.9b02903.
[45] Y. Ye, C. Wang, X. Zhang, Q. Hu, Y. Zhang, Q. Liu, D. Wen, J. Milligan, A. Bellotti, L. Huang, G. Dotti, Z. Gu, A melanin-mediated cancer immunotherapy patch, Sci Immunol 2 (17) (2017), https://doi.org/10.1126/sciimmunol.aan5692.